

Muscle stem cells contribute to long-term tissue repletion following surgical sepsis

Rebecca E. Schmitt^{1,2,3}, Aneesha Dasgupta^{1,2,3}, Paige C. Arneson-Wissink¹, Srijani Datta⁴, Alexandra M. Ducharme¹ & Jason D. Doles^{1,2,3*} 

¹Department of Biochemistry and Molecular Biology, Mayo Clinic, Rochester, MN, USA; ²Department of Anatomy, Cell Biology, and Physiology, Indiana University School of Medicine, Indianapolis, IN, USA; ³Indiana Center for Musculoskeletal Health, Indianapolis, IN, USA; ⁴Eden Prairie High School, Eden Prairie, MN, USA

Abstract

Background Over the past decade, advances in sepsis identification and management have resulted in decreased sepsis mortality. This increase in survivorship has highlighted a new clinical obstacle: chronic critical illness (CCI), for which there are no effective treatment options. Up to half of sepsis survivors suffer from CCI, which can include multi-organ dysfunction, chronic inflammation, muscle wasting, physical and mental disabilities, and enhanced frailty. These symptoms prevent survivors from returning to regular day-to-day activities and are directly associated with poor quality of life.

Methods Mice were subjected to cecal ligation and puncture (CLP) with daily chronic stress (DCS) as an *in vivo* model to study sepsis late-effects/sequelae on skeletal muscle components. Longitudinal monitoring was performed via magnetic resonance imaging, skeletal muscle and/or muscle stem cell (MuSCs) assays (e.g., post-necropsy wet muscle weights, minimum Feret diameter measurements, *in vitro* MuSC proliferation and differentiation, number of regenerating myofibres and numbers of Pax7-positive nuclei per myofibre), post-sepsis whole muscle metabolomics and MuSC isolation and high-content transcriptional profiling.

Results We report several findings supporting the hypothesis that MuSCs/muscle regeneration are critically involved in post-sepsis muscle recovery. First, we show that genetic ablation of muscle stem cells (MuSCs) impairs post-sepsis muscle recovery (maintenance of 5–8% average lean mass loss compared with controls). Second, we observe impaired MuSCs expansion capacity and morphological defects at 26 days post-sepsis compared with control MuSCs ($P < 0.001$). Third, when subjected to an experimental muscle injury, sepsis-recovered mice exhibited evidence of impaired muscle regeneration compared with non-septic mice receiving the same muscle injury (CLP/DCS injured mean minimum Feret is 92.1% of control injured, $P < 0.01$). Fourth, we performed a longitudinal RNA sequencing study on MuSCs isolated from post-sepsis mice and found clear transcriptional differences in all post-sepsis samples compared with controls. At Day 28, CLP/DCS mice satellite cells have multiple altered metabolic pathways, such as oxidative phosphorylation, mitochondrial dysfunction, sirtuin signalling and oestrogen receptor signalling, compared with controls ($P < 0.001$).

Conclusions Our data show that MuSCs and muscle regeneration are required for effective post-sepsis muscle recovery and that sepsis triggers morphological, functional, and transcriptional changes in MuSCs. Moving forward, we strive to leverage a more complete understanding of post-sepsis MuSC/regenerative defects to identify and test novel therapies that promote muscle recovery and improve quality of life in sepsis survivors.

Keywords sepsis; muscle stem cells; satellite cells; muscle wasting; skeletal muscle; muscle regeneration

Received: 17 August 2022; Revised: 18 January 2023; Accepted: 3 February 2023

*Correspondence to: Jason D. Doles, Department of Anatomy, Cell Biology, and Physiology, Indiana University School of Medicine, 635 Barnhill Drive, MS 334, Indianapolis, IN 46202, USA. Email: jadoles@iupui.edu

Introduction

Sepsis is defined as a detrimental host response to infection that causes life-threatening organ dysfunction.¹ An estimated 48.9 million people are affected by sepsis—a staggering number that is associated with roughly 20% of the worldwide death toll.² In addition to initial life-threatening complications, ~50% of all sepsis patients enter a chronic critical illness (CCI) state, which is defined by a >14-day stay in intensive care unit (ICU) and continued organ dysfunction.³ Unfortunately, the 6-month survival rate of patients in CCI is only 63%,³ indicating that the initial sepsis infection is not the only hurdle facing sepsis patients/survivors. Gentile and colleagues⁴ defined the host of long-term consequences plaguing CCI patients as PICS, or persistent inflammation, immunosuppression and catabolism syndrome. PICS is now a well-established phenomenon, believed to be a driving factor in negative long-term patient outcomes,^{3,5} and recognized as being particularly pervasive in the elderly sepsis patient population.⁶ Long-term outcomes include increased morbidity, muscle wasting and weakness, increased cognitive dysfunction, extended stays in long-term care facilities, and financial and emotional stress.⁷

Quality of life is an important measure for determining the total effects of an illness or injury on patients. Studies show that severely septic patients exhibit a significantly decreased quality of life (physically, mentally and/or health-related) from short-term to multiple years post incident.^{8–10} For example, one study utilized the EQ-5D to measure quality of life parameters of 580 patients from the ACCESS cohort¹¹ who were functionally independent before their diagnosis of severe sepsis.¹² Yende *et al.*¹² found that after 6 months, 37.5% of patients reported problems with overall mobility, 43.7% with usual activities, and 20.5% with self-care. The high prevalence of impaired mobility in sepsis survivors suggests a major role of sepsis associated muscle wasting in long-term patient functioning and recovery.^{13,14} In addition, muscle wasting resulting from sepsis has been associated with sepsis mortality,¹⁵ and interventions/rehabilitation for muscle wasting have been proposed as a strategy to improve patient outcomes.¹⁶

Adult skeletal muscle is capable of regeneration in response to injury, disease, exercise or normal daily use/wear-and-tear.¹⁷ One key driving force underlying robust life-long regenerative potential is the muscle stem cell, or satellite cell. Satellite cells maintain their position on the periphery of myofibres in a quiescent state until activation. They undergo asymmetric division, whereby daughter cells either continue towards terminal lineage differentiation or repopulate the satellite cell pool.¹⁷ Studies show that impaired satellite cell function or depleted satellite cell number negatively contributes to a wide variety of diseases and aging.^{18–20} Successful targeting of muscle regeneration via satellite cell interventions can improve muscle function in mouse models of

Duchenne muscular dystrophy²¹ and sarcopenia.²² Additionally, several animal sepsis studies report atrophy of gastrocnemius (GR),²³ tibialis anterior (TA)²⁴ and soleus²⁴ muscles, solidifying the notion that understanding whether skeletal muscle satellite cells are required for post-sepsis muscle recovery and/or whether sepsis affects this population of cells has the potential for broad impact. To date there are no treatments available to prevent progression or increase quality of life parameters/mobility in patients suffering from CCI/PICS after sepsis. Accordingly, targeting muscle stem cells holds promise as a potential therapeutic strategy to improve patient day-to-day activity, job maintenance and self-care for patients suffering from the long-term consequences of sepsis.

In this study, we utilized the cecal ligation and puncture/daily chronic stress (CLP/DCS) mouse model of surgical sepsis to closely recapitulate the human condition.²⁵ Our main goal was to address whether satellite cells contributed to long-term sepsis recovery of lean mass. To this end, we (i) longitudinally characterized lean muscle loss in mice post CLP, (ii) utilized a genetic mouse model to establish the necessity of satellite cells in lean mass recovery following surgical sepsis, (iii) demonstrated that satellite cell number is decreased in post-sepsis mice, (iv) leveraged *in vitro* studies to highlight proliferative and morphological defects of satellite cells harvested from recovered septic mice, (v) showed that post-septic mice exhibit persistent deficits in muscle regeneration and (vi) report widespread satellite cell transcription changes that do not appear to be caused by myofibre type-switching or as a compensatory mechanism to changes in whole muscle metabolism. Understanding the both the role of satellite cells in muscle recovery and the effect of sepsis on this cell population will hopefully lead to novel therapeutic strategies for formally septic patients suffering from PICS/CCI.

Methods

Animals

All animal protocols were approved by the Mayo Clinic Institutional Animal Care and Use Committee (IACUC) and performed at Mayo Clinic. C57BL/6J mice (catalog #000664) were purchased from Jackson Laboratory. All mice used in these studies were housed, and the Pax7-DTA (Pax7^{CreERT2}; R26R^{DTA})²⁶ mice were bred, according to NIH guidelines for the ethical treatment of animals in a pathogen-free facility at Mayo Clinic (Rochester, MN) for a minimum of two weeks before the start of the experiment. For induction of satellite cell ablation in Pax7-DTA mice, intraperitoneal injection was used to deliver 2-mg tamoxifen (TRC) in corn oil (Sigma) or vehicle (corn oil) daily, for five consecutive days. All animals

in this study were female, apart from the Pax7-DTA study (Figures 2 and S4–S5), and 7 months of age at time of surgery. Mice for the Pax7-DTA investigation were male and between 6 and 7 months of age at surgery.

Cecal ligation and puncture and daily chronic stress (DCS)

Procedures were performed essentially as described previously,²⁵ with slight modifications, and by following the Minimum Quality Threshold in Preclinical Sepsis Studies (MQTiPSS)²⁷ criteria. Briefly, mice were anesthetized using isoflurane (Pirmal). The cecum was extracted from the abdomen and ligated 1.0 cm from the tip. One hole was punctured at the end of the cecum with a 25-G (BD Biosciences) needle, faecal matter released, and the cecum returned to the abdomen. All mice prior to surgery received 0.5-mg/kg buprenorphine SR-LAB (ZooPharm 0.5 mg/mL) and 4 mg/kg Meloxicam SR (ZooPharm 2 mg/mL). Post-surgery, CLP mice received intraperitoneal injection of antibiotics (25 mg/kg of imipenem monohydrate (LKT Labs or Med Chem Express) and 1-mL warmed saline (BD) subcutaneously for resuscitation. Antibiotics were continued to be delivered two times per day, for 72 h. The first day post-surgery was used as a recovery day, and starting the second day post-surgery, mice underwent DCS using immobilization tubes (Kent Scientific) for 2h/day, for seven consecutive days. Mice were monitored for health and wellness throughout experiment. One mouse from the Day 8 time point did not receive DCS on the first day (received DCS same as rest of the mice until endpoint) as it demonstrated distress, but not meeting humane end point criterion. EchoMRI body composition analysis (Echo Medical Systems) was used for determination of lean and fat mass. In rare instances when a CLP/DCS mouse did not demonstrate a decrease in lean mass (defined as lean mass $\geq 100\%$ from baseline), it was excluded from further analyses.

Serum levels of C-reactive protein and aspartate aminotransferase activity

At time of harvest, cardiac puncture was used to collect blood, placed in lithium heparin tubes (BD), and centrifuged at 13 000 RPM for 10 min. Serum was collected and stored at -80°C until use. Mouse C-reactive protein (CRP) was measured using a quantikine enzyme-linked immunosorbent assay (ELISA, R&D System) and aspartate aminotransferase (AST) activity was determined via a colorimetric assay (Sigma), both according to the respective manufacturer protocols.

Immunofluorescence

The TA muscle was harvested from all mice and placed in a 30% sucrose sink overnight at 4°C . TAs were embedded in O.C.T (Tissue-Tek) and cut in $8\text{-}\mu\text{m}$ sections. All sections were fixed using 4% paraformaldehyde solution (Thermo Fisher) for 15 min at room temperature and washed twice ($\times 2$) with Dulbecco's phosphate-buffered saline (DPBS) (PBS—Gibco). Permeabilization was performed using 0.5% Triton X-100 (Sigma) in PBS for 5 min at room temperature (RT), then washed $\times 2$ in immunofluorescence buffer (IFB: 3% bovine serum albumin [BSA, GoldBio], 0.2% Triton X-100 (Sigma), 0.2% Tween-20 [Sigma], in PBS). Sections were blocked with IFB for 60 min at RT. MF-20 (DSHB) was diluted 1:2 and laminin (Sigma) 1:250 in IFB and sections incubated overnight at 4°C . The following morning, sections were washed $\times 2$ with IFB and incubated with secondary antibody, anti-mouse Alexa Fluor 488 and anti-rabbit Alexa Fluor 647 (Invitrogen), at a 1:250 dilution in IFB for 45 min at RT. Sections were washed $\times 2$ with IFB and incubated with DAPI (1:1000) diluted in IFB for 10 min, washed $\times 2$ with PBS and Mowiol (EMD Millipore) used for mounting. Images were taken with the Hamamatsu ORCA-Flash 4.0 LT CMOS camera using Nikon NIS-Elements. MyoVision v1.0 (<https://www.uky.edu/chs/center-for-muscle-biology/myovision>,²⁸) was used for minimum Feret diameter calculations. Each biological replicate (represented as a single point on graph) contains minimum Feret diameters from three images per sample.

Myofibre typing

TA sections were prepared as above. Sections were blocked for 1 h at RT with the mouse-on-mouse blocking reagent (Vector Laboratories). Sections were washed $\times 2$ with PBS and incubated with BA-D5 (type I myofibres, supernatant, 1:100, DSHB), SC-71 (type IIa myofibres, supernatant, 1:100, DSHB), BF-F3 (type IIb myofibres, concentrate, 1:100, DSHB), and laminin (1:250, Sigma) diluted in 1% BSA at 37°C for 45 min. Sections were washed $\times 2$ with PBS and incubated with the following Alexa Fluor secondary antibodies (Invitrogen), diluted 1:250 in 1% BSA, at 37°C for 35 min: anti-mouse IgG2b-405, anti-mouse IgG1-488, anti-mouse IgM-594, and anti-rabbit IgG-647. Sections were washed with PBS $\times 2$, mounted with Mowiol and imaged at $\times 4$ using the Hamamatsu ORCA-Flash 4.0 LT CMOS camera using Nikon NIS-Elements. ImageJ²⁹ cell counter was used to manually assess myofibre types for quantification. All TA sections were negative for type I myofibres and were therefore not included in the myofibre typing quantification graph in Figure 1F.

Satellite cell isolation, culture, proliferation and differentiation

Satellite cell isolation was performed as previously described.³⁰ Briefly, all hindlimb muscles were harvested, minced and dissociated using 0.2% collagenase II (Gibco) with agitation at 37°C for 1 h. Digested samples underwent straining to remove nondigested/large objects. A Satellite Cell Isolation Kit (Miltenyi) was used following manufacturing instructions to isolate satellite cells. Once isolated, satellite cells were grown in growth media containing DMEM/F12 (Gibco) plus 20% foetal bovine serum (FBS—Gibco), 10% horse serum (HS—Gibco), 1% chick embryo extract (Life Science Production), 1% penicillin–streptomycin (PenStrep—Gibco), 0.1% Amphotericin B (Corning) and 0.2% Fibroblast Growth Factor 2 (GoldBio). Satellite cells were maintained at 37°C and 5% oxygen. To assess proliferation, cells were plated at 500 cells per square centimetre and 1000 cells per square centimetre and maintained in growth media until spontaneous differentiation. Myogenic differentiation was performed by seeding wells at 1000 cells per square centimetre and given differentiation media containing DMEM/F12 with 2% HS and 1% PenStrep. Both proliferation and differentiation of cells was monitored by IncuCyte ZOOM (Essen BioScience) and their measures exported via masking analysis (exclusion of linear objects in proliferation studies, threshold: eccentricity <0.96) in IncuCyte ZOOM 2016B. Each biological replicate contains the average of eight replicate wells with four images per well.

RNAscope and Pax7 quantification

RNAscope was performed as described by the manufacturer (Advanced Cell Diagnostics, Inc. [ACD]) using the RNAscope 2.5 HD Assay-RED kit (Document Number 322360-USM) with minor modifications. Briefly, tissue sections were fixed with 4% PFA (Thermo) for 15 min at RT. Tissues were dehydrated in 5-min steps of 50% ethanol, 70% ethanol, 100% ethanol and second fresh 100% ethanol. Sections were pretreated with hydrogen peroxide (ACD) for 10 min at RT then RNAscope Protease IV (ACD) for 30 min at RT. 1X PBS was used to wash sections $\times 2$. Pax7, positive control, and negative control probes (ACD) were added to tissue sections and incubated at 40°C for 2 h. Slides were washed $\times 2$ with 1X wash buffer (ACD) and either continued with the protocol or paused overnight in 5X SSC (Sigma) at RT. Amplification Steps 1–6 occurred as stated in the manual, with the exception that AMP5 was incubated for 45 min. A 1:60 ratio of RED-B:RED-A (ACD) was added to all sections and incubated for 10 min at RT. Slides were stained with 50% haematoxylin (Sigma) and mounted with EcoMount (ACD). Images were taken with the Nikon DS-Fi3 camera using Nikon NIS-Elements. Pax7-positive nuclei were quantified manually and then divided

by the number of myofibres per image. Each biological replicate (represented as a single point on graph) is the average calculation of Pax7-positive nuclei per myofibre from four to six images.

RNA sequencing and analysis

Satellite cells were isolated as described above. Total RNA was extracted using TRIzol reagent (Invitrogen) and chloroform (Sigma) and isolation via the Qiagen RNeasy kit. Harvested satellite cells from two to three mice were pooled for each RNA sample. CLP/DCS Day 28 satellite cell data (Figures 5 and S8) were derived from cells isolated on Days 27 and 28, with Day 28 being used as the label. GENEWIZ, LLC, performed the library preparation and RNA sequencing to hit counts as follows: RNA concentration was determined using Qubit 2.0 Fluorometer (Life Technologies), RNA integrity scores with 4200TapeStation (Agilent Technologies), and rRNA depletion with Ribozero rRNA Removal Kit (Illumina). NEBNext Ultra RNA Library Prep Kit for Illumina (NEB) was used according to manufacturer's protocol. Sequencing was performed on the Illumina HiSeq using 2 \times 150 paired-end configuration. HiSeq Control Software was used for image analysis and base calling. FASTQ files were generated from the raw sequence data using Illumina's bcl2fastq 2.17 software. Reads were trimmed via Trimmomatic (v.0.36) and aligned to *Mus musculus* ENSEMBL genome via STAR aligner (v.2.5.2b). Subread package (v.1.5.2) with counts feature was used to calculate unique gene hit counts. We further converted hit counts to FPKM via Galaxy (<https://usegalaxy.org>).

TIBCO Spotfire Analyst 7.11.2.4 was used perform principal component analysis and calculate significant genes ($2 < \log_2FC < -2$, $P < 0.05$) between CLP/DCS Days 4, 8 and 28 versus control. Hierarchical clustering was performed utilizing those significant genes via clustering method: complete linkage and distance measure: correlation. Significant genes, found as described directly above between CLP/DCS Day 4 and control ($-1.75 > \log_2FC > 1.75$, $P < 0.05$), CLP/DCS Day 8 and control ($-2 > \log_2FC > 2$, $P < 0.05$) and CLP/DCS 28 and control ($-1.25 > \log_2FC < 1.25$, $P < 0.05$) were uploaded into ingenuity pathway analysis (IPA,³¹ v.70750971) to identify altered pathways.

Whole muscle metabolomics

A minimum of 40 mg of gastrocnemius muscle was sent to Metabolon Inc. for untargeted metabolomic analysis using an ultrahigh performance liquid chromatography-tandem mass spectroscopy unit according to their standardized pipeline. Statistical analyses from gastrocnemius metabolomics were performed by Metabolon using Student's *t*-test with

Welch's correction. Metabolites were uploaded to MetaboAnalyst 5.0³² to log transform and Pareto scale data to produce a 3D principal component analysis (PCA) plot, perform hierarchical clustering using the top 25 altered metabolites and identify altered metabolic pathways.

Statistical analyses

GraphPad Prism 9 (versions 9.0.0–9.3.0) were used for all statistical analyses. Student's *t*-tests were unpaired, and one- and two-way ANOVAs were performed with Bonferroni multiple comparisons (BMC). Minimum Feret values were analysed in pairwise comparisons using nonlinear regression. Survival data were analysed using Kaplan–Meier simple survival analysis. Significance was defined as $P < 0.05$, see legends for further detail. All numerical data are reported as mean \pm SEM, except for minimum Feret diameter measures which are mean \pm SD.

Results

Utilization of cecal ligation and puncture and daily chronic stress as a murine model of surgical sepsis results in loss of lean mass

The first goal of this study was to assess the extent of physiological changes in skeletal muscle that occur in the CLP/DCS mouse model. Mice underwent CLP surgery on Day 1, with baseline measurements on Day 0, followed by resuscitation with saline. Antibiotics were delivered after surgery and continued twice per day, for 3 days, to mimic in-patient treatment.²⁵ DCS was administered for 2 h every day, over 7 days, starting on Day 3 to mimic stress and lack of movement in ICU patients. In these cohorts, 100% of control mice and ~93% of CLP/DCS mice survived to the experimental endpoint of 27/28 days (Figure 1A) or in combined studies assessing acute survival, 100% control mice and ~82% of CLP/DCS mice (Figure S1A). To longitudinally monitor sepsis progression in our model, we measured serum levels of CRP (a marker of inflammation found to be increased in both mouse and human sepsis studies),^{33,34} and AST activity, an indicator of liver dysfunction found to be increased in both mouse and pig models of sepsis^{25,33,35} (Figure 1B). Both CRP and AST were increased at CLP/DCS Day 4 (+67.90 \pm 10.97% and +95.59 \pm 28.66%, respectively). At CLP/DCS Day 8, CRP levels were trending up (+26.19 \pm 10.97%, $P = 0.0692$) while AST levels were increased, but not statistically significant (+56.93 \pm 28.66%, $P = 0.166$). Interestingly, CRP levels dropped to control levels by CLP/DCS Day 28, while AST levels remained significantly elevated (+86.9 \pm 28.66%) (Figure 1B).

Maximum weight loss in CLP/DCS mice was at Day 5 (4 days post-CLP) with a decrease of 12.47 \pm 1.17% weight compared

with controls. CLP/DCS did not have a significantly decreased body weight compared with control mice by Day 26 (4.10 \pm 1.45%), demonstrating that CLP/DCS mice recovered to near baseline weight measurements (97.90%) (Figure S1B). We also evaluated longitudinal fat and lean mass by magnetic resonance imaging (EchoMRI) two times per week. During the first week, CLP/DCS mice lost the highest amount of lean mass at Day 3 (~10%) and fat mass at Day 7 (~59%) compared with baseline values (Figures 1C and S1C, respectively). CLP/DCS mice maintained a significant loss of lean mass at Day 10 (~8%) and by the fourth week, Day 26, of recovery from CLP/DCS, mice recovered to near baseline measurements of lean and fat mass (97.5% and +6.4%, respectively). To address whether CLP, versus DCS, was the largest contributor to the response demonstrated in the results above, we also assessed a CLP only group in conjunction with the previous study (Figure S2, contains data found in Figures 1A, C–D and S1B–D). CLP and CLP/DCS outcomes were largely similar with respect to survival (Figure S2A), body mass (Figure S2B), and fat mass (Figure S2C). Of note, post-sepsis recovery of lean mass from CLP/DCS mice was more protracted when compared to CLP alone (recovery by Day 13 versus Day 10, Figure S2D).

Harvested wet weights of CLP/DCS tibialis anterior (TA), gastrocnemius (GR), and fat pad (fat) were evaluated at Days 4, 8 and 28. All values were normalized to baseline body weight to account for any variation in mouse size (baseline body mass and raw wet masses can be found in Figure S3). All three groups were reduced in CLP/DCS mice at Day 4 when compared with control: TA mass was decreased by 27.52 \pm 5.71%, GR by 25.79 \pm 10.67% ($P = 0.06$) and fat by 41.30 \pm 11.29%. CLP/DCS Day 8 GR was decreased by 12.02 \pm 10.91% compared with controls but was not statistically different, nor was it by experimental endpoint (15.38 \pm 10.67%). At Day 8, CLP/DCS mice maintained a significantly decreased TA mass (18.33 \pm 5.84%), but not by Day 28 (7.020 \pm 5.52%, Figure 1D). Fat mass was significantly decreased at both CLP/DCS Days 8 and 28 (66.03 \pm 11.55% and 41.78 \pm 10.88%, respectively) versus controls (Figure S1D). Little difference was noted between CLP/DCS and CLP harvested wet weights of TA, GR and fat mass (Figure S2E).

Consistent with decreased TA mass, TA cross-sections stained for laminin and nuclei demonstrated visual differences in myofibre size at CLP/DCS Day 8 (Figure 1E—top). MyoVision-based myofibre quantification of minimum Feret diameter confirmed these observations, whereby CLP/DCS Day 8 TAs were significantly reduced in size compared with all other CLP/DCS time points and control (Figure 1E—bottom). Lastly, myofibre typing of TA cross-sections was performed and stained for laminin, type I, type IIa, type IIb and type IIx (unstained) myofibres. TA sections contained no type I myofibres but demonstrated an increase in type IIb myofibres in CLP/DCS Day 4, a trend at Day 8

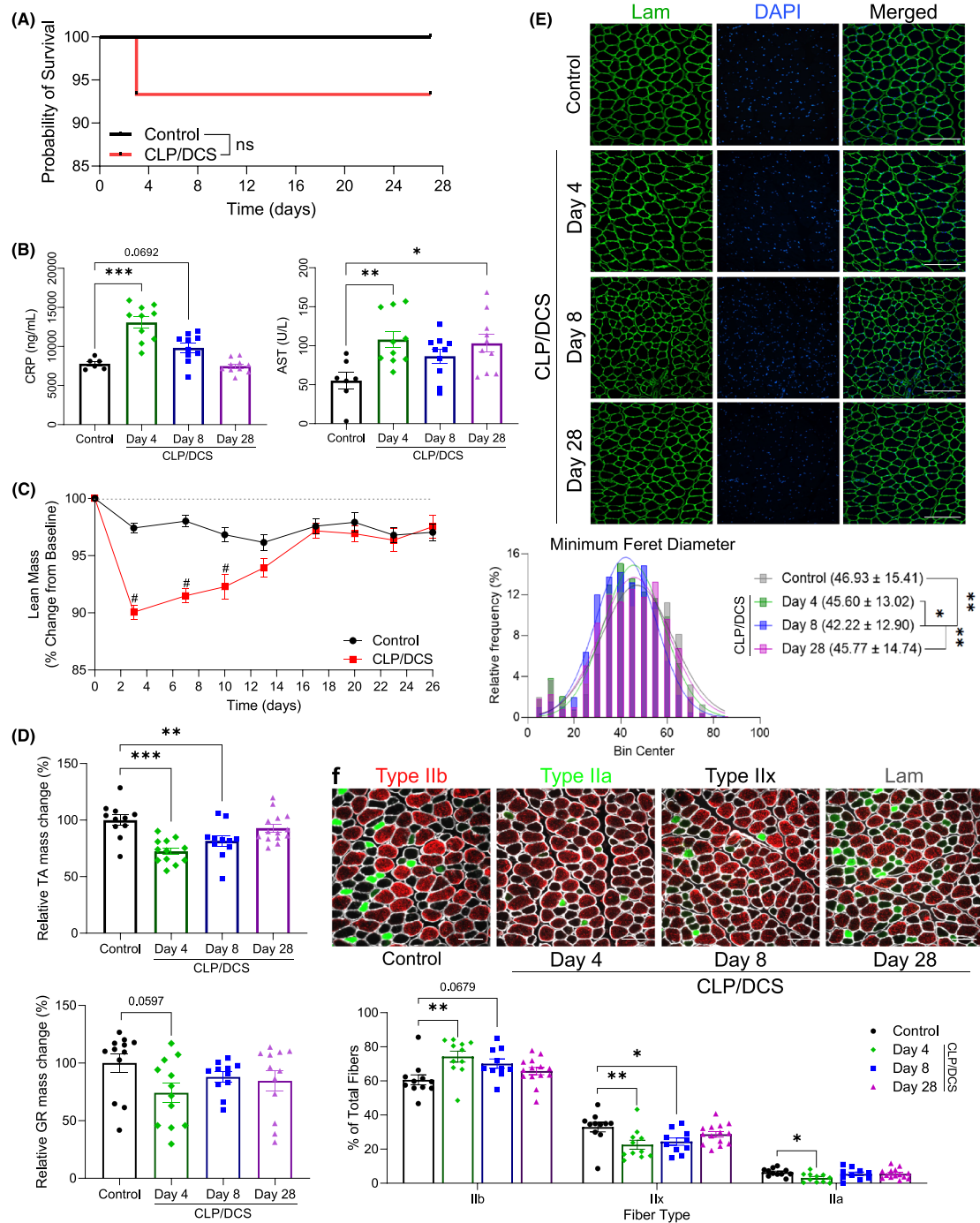


Figure 1 Characterization of muscle loss and recovery in CLP/DCS mice. (A) Combined cecal ligation and puncture (CLP)/daily chronic stress (DCS) Kaplan–Meier survival curve versus control mice to experiment endpoint. (B) Serum levels of mouse C-reactive protein (CRP) and aspartate aminotransferase (AST) activity. (C) Control and CLP/DCS percentage change from baseline in lean mass. Data from mouse MRI on Day 3 or 4 are represented on lean mass graph as Day 3. (D) Harvested wet weights, as change in percentage of control, of tibialis anterior (TA, top) and gastrocnemius (GR, bottom) normalized to baseline body weight, respectively, in control and CLP/DCS Days 4, 8 and 28. (E) Immunofluorescence images (top) and quantification of minimum Feret diameter (bottom) of tibialis anterior (TA) cross-sections from control, Days 4, 8 and 28 CLP/DCS mice. Green = laminin, Blue = DAPI. Images are representative and $\times 20$ with scale bar = 200 μm . See Table S1 for all P value comparisons. (F) Immunofluorescence images (top) and quantification (bottom) of tibialis anterior (TA) myofibre typing from control, Days 4, 8 and 28 CLP/DCS mice. Red = type IIb, Green = type IIa, Unstained = type IIx, White = laminin. Images are representative and $\times 20$ with scale bar = 100 μm . Data from muscle mass/minimum Feret diameter/myofibre typing were harvested on Day 27 or 28 and are labelled as Day 28. B = log-rank test. C, E, G = One-way ANOVA with Bonferroni multiple comparisons (BMC). D = Two-way ANOVA with BMC. F = nonlinear fit pairwise comparisons. Significance: * $P < 0.05$, **/ $\&P < 0.01$, ***/ $\#P < 0.001$. (B) $n = 12\text{--}13$. (C–D) $n = 16\text{--}45$. (E) $n = 11\text{--}14$. (F) $n = 5$. (G) $n = 10\text{--}14$. Each $n =$ one mouse.

($13.61 \pm 3.92\%$ and $9.50 \pm 4.01\%$, respectively), a decrease in type IIx fibres in CLP/DCS Days 4 and 8 mice ($10.34 \pm 3.29\%$ and $8.52 \pm 3.37\%$, respectively) and a decrease in type IIa fibres at CLP/DCS Day 4 ($3.27 \pm 1.20\%$) versus control (Figure 1F).

Satellite cells are required for post-surgical sepsis muscle recovery

Lean mass was significantly decreased in CLP/DCS mice, but near complete lean mass recovery/regeneration was observed by the end of 2 weeks post-CLP (Figure 1). As muscle stem cells, or satellite cells, have been previously shown to be necessary for muscle regeneration,²⁶ we wanted to determine whether the muscle stem cell population was necessary for this recovery in post-surgical sepsis mice. We utilized the established Pax7-DTA mouse model to allow for genetic ablation of Pax7 expressing cells upon tamoxifen administration.²⁶ Mice were separated into four groups, control or CLP/DCS treated with either vehicle or tamoxifen and allowed a washout period of 10 days before proceeding with CLP/DCS (Figure 2A). We noted little difference in experimental survival between CLP/DCS vehicle and tamoxifen groups (Figure S4A). Longitudinal body weight studies revealed that both CLP/DCS groups lost a significant amount of body weight over the first few days post-surgery. By Day 8, the CLP/DCS groups recovered enough body weight to reach non-significance but maintained a lower mass trend throughout the rest of the experimental timeline (Figure S4B). EchoMRI scans revealed CLP/DCS vehicle treated mice lost ~6–8% lean mass compared with controls in the first week post-surgery, but rapidly gained lean mass between Days 7 and 10 and maintained lean mass throughout the remainder of the experimental timeframe (Figure 2B, purple vs. orange and grey lines). Strikingly, CLP/DCS tamoxifen treated mice lost ~8.5–11% lean mass in the first week and maintained an ~5–8% lean mass loss throughout the experiment when compared with control groups (Figure 2B, green vs. orange and grey lines). Both CLP/DCS groups lost between ~55% and 70% fat mass on Day 4, followed by recovery of fat mass from Days 4 to 19 to where no statistical differences were detected in CLP/DCS groups versus controls (Figure S4C).

TA muscle cross-sections were stained for laminin and DAPI and minimum Feret diameter quantified across groups (Figure 2C). While no differences were observed between control groups (difference of 1.2), CLP/DCS tamoxifen had a significantly reduced minimum Feret diameter compared with CLP/DCS vehicle (difference of 3.9), control vehicle mice (difference of 2.78) and trending versus control tamoxifen mice ($P = 0.056$, difference of 1.58) (Figure 2C—bottom). We next queried whether post-necropsy TA, GR or fat mass was altered between groups (baseline body

mass and raw wet masses can be found in Figure S5). Although there were no significant differences in TA wet weights when normalized to baseline body weight, there was a trend in progression of decreased weight, where control vehicle > control tamoxifen > CLP/DCS vehicle > CLP/DCS tamoxifen (Figure S4D). CLP/DCS tamoxifen mice did exhibit significantly reduced GR weight when compared with control vehicle ($20.73 \pm 6.14\%$), with no other significant differences between groups (Figure S4E). CLP/DCS tamoxifen mice had significantly decreased fat mass compared with the CLP/DCS vehicle group ($65.62 \pm 20.49\%$) but not versus control vehicle or control tamoxifen (Figure S4F). To validate that the phenotype of impaired muscle recovery was due to satellite cell reduction (not necessarily a complete ablation of the satellite cell population), we used RNA *in situ* hybridization (RNAscope) to identify (Figure 2D—top) and quantify Pax7-positive cells/nuclei (Figure 2D—bottom). The control vehicle group had significantly more Pax7-positive nuclei per myofibre compared with all other groups. No differences in the number of Pax7-positive cells were seen between control tamoxifen, CLP/DCS vehicle and CLP/DCS tamoxifen groups (Figure 2D—bottom).

Primary satellite cells isolated from recovered CLP/DCS mice have altered proliferation and morphological characteristics

We next aimed to assess the ability of satellite cells to proliferate and differentiate (two main functional stem cell hallmarks) when harvested from previously septic mice. We harvested primary muscle stem cells from control or CLP/DCS mice at Days 4 and 26 post-procedure. Proliferating CLP/DCS Day 4 satellite cells exhibited increased proliferation dynamics as evidenced by changes in field confluence (fold change 4.18 ± 0.82) (Figures 3A, B—left) and object count (fold change 1.93 ± 0.52) (Figure 3B—middle), with no change in average object area (Figure 3B—right) when compared with control cells at 56 h post-isolation. We found no difference in the fold change of confluence in satellite cells isolated from CLP/DCS mice at Day 26 (Figures 3C, D—left). We did however observe that by the 40-h mark, the number of CLP/DCS Day 26 cells declined (Figure 3D—middle) whereas the average area increased (Figure 3D—right) compared with control cells.

There were no significant differences in satellite cell differentiation parameters measured (confluence, object count and average area) at either Day 4 or Day 26 in CLP/DCS satellite cells compared with controls (Figures S6A, B). Furthermore, we evaluated myotube morphology from differentiated satellite cells and found that Day 4 CLP/DCS myotubes had an increase in myotube width, but not length, while Day 26 CLP/DCS myotubes had no difference in width but

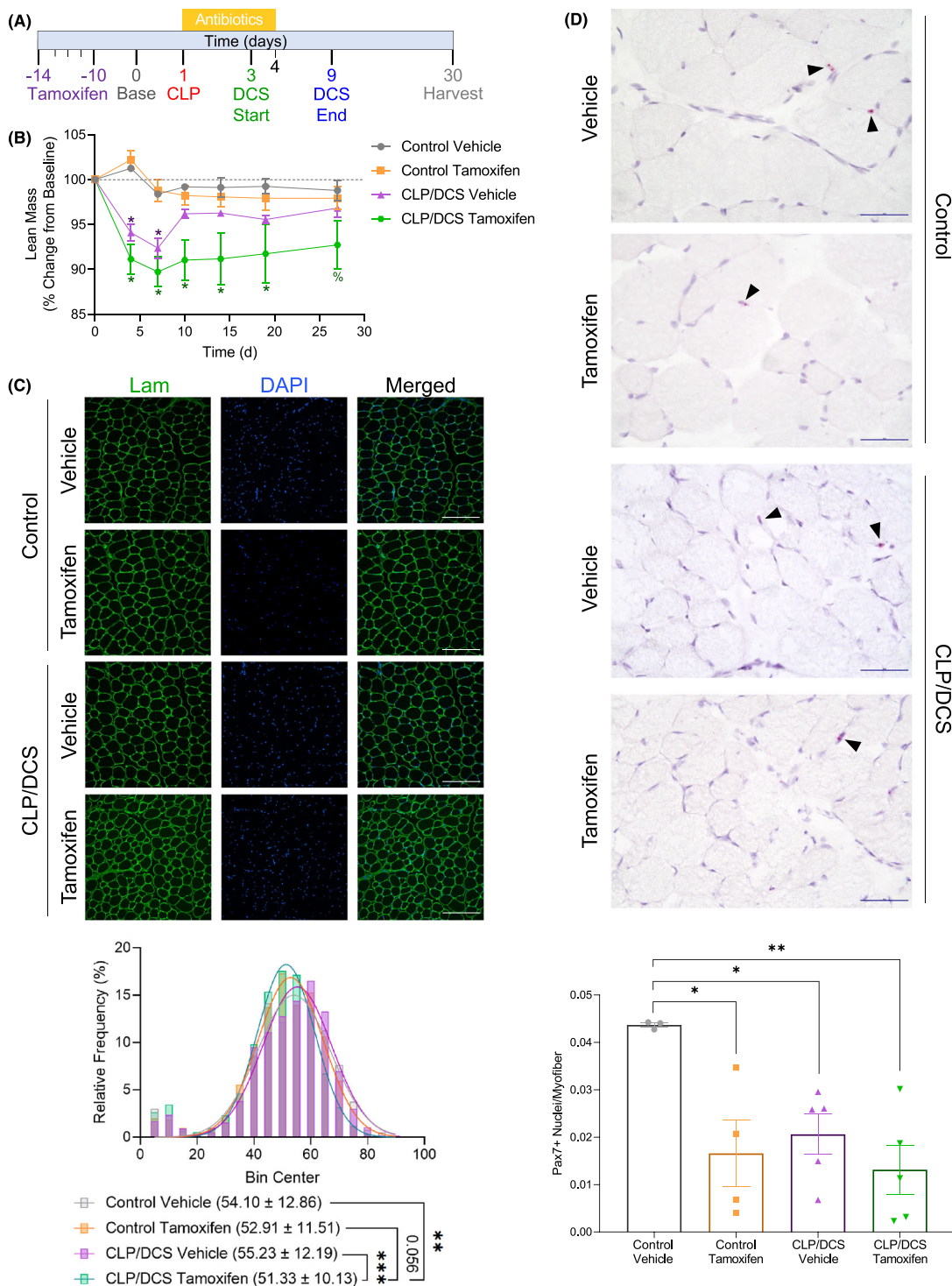


Figure 2 Satellite cell reduction reduces muscle regeneration capacity in cecal ligation and puncture/daily chronic stress (CLP/DCS) mice. (A) Timeline representing male Pax7-DTA mice treated for five consecutive daily injections of tamoxifen or vehicle, 15 days before surgery. Percentage change from baseline of (B) lean mass. (C) Immunofluorescence images (top) and quantification of minimum Feret diameter (bottom) of tibialis anterior (TA) cross sections from either vehicle or tamoxifen control and CLP/DCS mice. Green = laminin, Blue = DAPI. Images are $\times 20$ with scale bar = 200 μm . (D) Pax7 staining (top) and quantification of Pax7-positive nuclei per myofiber (bottom) of tibialis anterior (TA) cross-sections from vehicle or tamoxifen control and CLP/DCS mice. Purple = haematoxylin (nuclei), Red = Pax7. Images are $\times 40$ with scale bar = 50 μm . All images are representative. B = Two-way ANOVA with Bonferroni multiple comparisons (BMC) where *significant vs. control vehicle and control tamoxifen, ^significant vs. control tamoxifen, and % significant vs. control vehicle, $P < 0.05$. C = nonlinear fit pairwise comparisons. D = One-way ANOVA with BMC where significance = * $P < 0.05$, ** $P < 0.01$, *** $P < 0.001$. See Tables S4 and S5 for all P values from all comparisons in (B) and (C), respectively. $N = 3-7$. Each $n =$ one mouse.

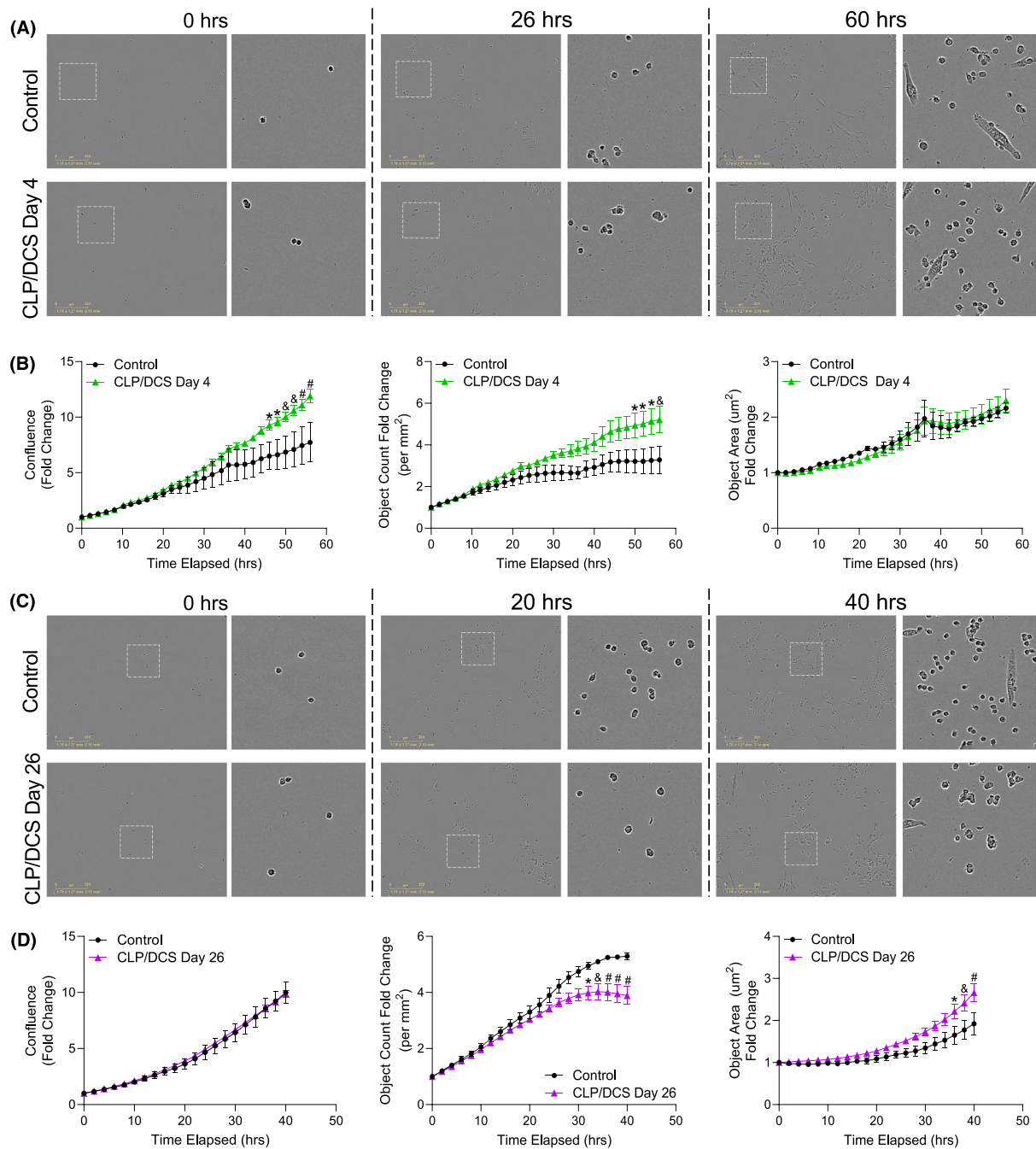


Figure 3 Satellite cells from cecal ligation and puncture/daily chronic stress (CLP/DCS) mice demonstrate intrinsic alterations in proliferation based on time post-sepsis infection. (A, B) Muscle stem cell (MuSC) measurements of proliferation from control and CLP/DCS Day 4 mice. (A) Representative images of time 0, 26 h and 60 h of proliferation. Left image is $\times 10$ with location of inset box (white dashed square). Right image is inset. (B) Quantification over time of MuSC (left) confluence, (middle) object count and (right) object area. (C, D) Control and Day 26 CLP/DCS proliferation measurements of MuSCs. (C) Representative images of time 0, 20 h and 40 h of proliferation. Left image is $\times 10$ with location of inset box (white dashed square). Right image is inset. (D) Quantification over time of MuSC (left) confluence, (middle) object count and (right) object area. All $\times 10$ images are representative with scale bar = $300 \mu\text{m}$. B and D = One-way ANOVA with Bonferroni multiple comparisons (BMC) where significance is * $P < 0.05$, & $P < 0.01$, # $P < 0.001$. Day 4 (B), $n = 3$ –5. Day 26 (D), $n = 2$ –5. Each $n =$ satellite cells isolated from a single mouse.

had a trend towards increased myotube length when compared with controls (Figures S6C, D). Taken together, satellite cells isolated from previously septic mice exhibit functional

and morphometric differences when compared with control cells—differences that appear to be related to timing of post-sepsis isolation/analysis.

Secondary injury/insult reveals an impaired muscle regeneration response in previously septic mice

Given (1) observations that satellite cells are required for optimal muscle recovery post-sepsis and (2) *in vitro* data suggesting morphological/functional defects in Day 26 satellite cells, we next asked if muscle regeneration is compromised in previously septic mice. On Day 23 (22 days post-CLP surgery), mice received an intramuscular injection of either barium chloride (BaCl₂; injury) or saline (vehicle) in the TA muscle (Figure 4A). Injured (or control) muscles were harvested on Day 50 (28 days post-BaCl₂/chemical injury) and sectioned and stained for laminin and DAPI to quantify myofibre widths. We observed morphological differences in myofibre shape and size when visually comparing control or CLP/DCS vehicle and injury groups (Figure 4B—top). Minimum Feret diameter quantification by MyoVision confirmed that the CLP/DCS injury group had a significantly decreased mean compared with all other groups (Figure 4B—bottom).

We next wanted to determine whether MuSCs were able to expand in injured post-sepsis mice. RNAscope was used to identify Pax7-positive nuclei (Figure 4C—top) and quantification revealed a modest (53%), though not statistically significant, reduction in Pax7-positive nuclei per myofibre in CLP/DCS vehicle treated mice compared with control vehicle mice (0.019 vs 0.041 Pax7-positive nuclei per myofibre, respectively) (Figure 4C—bottom). At experimental endpoint (Day 50), control vehicle and control injury mice did not exhibit differences in Pax7 cell number. There was, however, an increase in Pax7-positive nuclei per myofibre in CLP/DCS injury versus CLP/DCS vehicle treated mice (Figure 4C—bottom). Furthermore, quantification of the number of regenerating myofibres was performed to further assess potential differences in tissue regeneration. There was no significant difference in the percentages of regenerating myofibres between control and CLP/DCS vehicle or injury mice, although there was a trend towards fewer regenerating myofibres in the injury CLP/DCS vs control injury groups (Figure S7A). In addition, there were no differences in the number of centrally located nuclei in regenerating myofibres in control vs CLP/DCS mice in either vehicle or injured mice (Figures S7B, C).

Transcriptome analyses of satellite cells isolated from previously septic mice reveal persistent alterations in cellular metabolism

We next performed transcriptome (RNA-sequencing) analyses of freshly isolated satellite cells from control and CLP/DCS mice at Days 4, 8, and 28 to better understand molecular changes associated with observed functional deficits. PCA across all samples and transcripts demonstrated clear clustering of CLP/DCS Day 4 (red) and Day 8 (purple) samples away

from controls (blue), while CLP/DCS Day 28 (yellow) and control samples appear more closely related/overlapping in 2D PCA space (Figure 5A). Hierarchical clustering (HCC) analysis revealed two main branches, of which controls were grouped under one branch while the majority of sepsis samples grouped under the second branch (all but one Day 28 CLP/DCS sample). In the second main branch, each CLP/DCS sample clustered well based on time point (Figure 5B). Comparison of differentially expressed genes (DEGs) across all CLP/DCS time points versus control (see Figure S8 for top DEGs per CLP/DCS time point) indicated little overlap between Day 28 and Days 4 and 8. Conversely, Days 4 and 8 exhibited substantial overlap in DEGs, but also maintained a high number of unique genes at each time point (Figure 5C).

Utilizing IPA, we assessed altered biological pathways between the control and CLP/DCS Day 4 (Table S7), Day 8 (Table S8) and Day 28 (Table S9) samples. As we were initially interested in the long-term effects of sepsis on satellite cells, we focused on the top 25 altered pathways between CLP/DCS day 28 versus control, of which many were metabolism-focused pathways. Further, there was significant overlap between transcripts associated with each of the top 4 altered pathways (i.e., oxidative phosphorylation, mitochondrial dysfunction, sirtuin signalling pathway, and oestrogen receptor signalling, Figure 5D)—alterations that persisted in CLP/DCS Day 28 satellite cells versus control cells (Figure 5E). These transcripts, including *Ndufa6*, *Ndufb8*, *Ndufb11*, *Sdhb*, *Sdhc*, *Sdhd*, *Cyc1*, *Uqcrc2*, *Cox4i1*, *Cox7b*, *Atp5d* and *Atp5e*, are all integral for functioning of mitochondrial complexes 1–5 in oxidative phosphorylation and are top candidates as mediators of long-term, post-sepsis satellite cell dysfunction and impaired muscle regeneration.

Whole muscle metabolomics from post-septic mice do not reveal persistent mitochondrial metabolism-related defects

Our results above suggest a sustained increase in components necessary for oxidative phosphorylation, across all five mitochondrial complexes, in satellite cells after sepsis induction via CLP/DCS. We next sought to query whole muscle metabolism to better understand the global/macroenvironment context in which satellite cells reside. GR muscle from control, CLP/DCS Days 4, 8 and 28 mice underwent untargeted metabolomic profiling. 3D PCA analysis using all metabolic signatures revealed similar clustering trends as those observed via satellite cell RNA sequencing, where more overlap was seen between control and CLP/DCS Day 28 samples, while CLP/DCS Days 4 and 8 clustered distinctly (Figure 6A). HCC utilizing the top 25 altered metabolites revealed two main branches, one containing the control and CLP/DCS Day 28 samples and the second containing the CLP/DCS Days 4 and 8 samples (Figure 6B). Interestingly, numerous metabo-

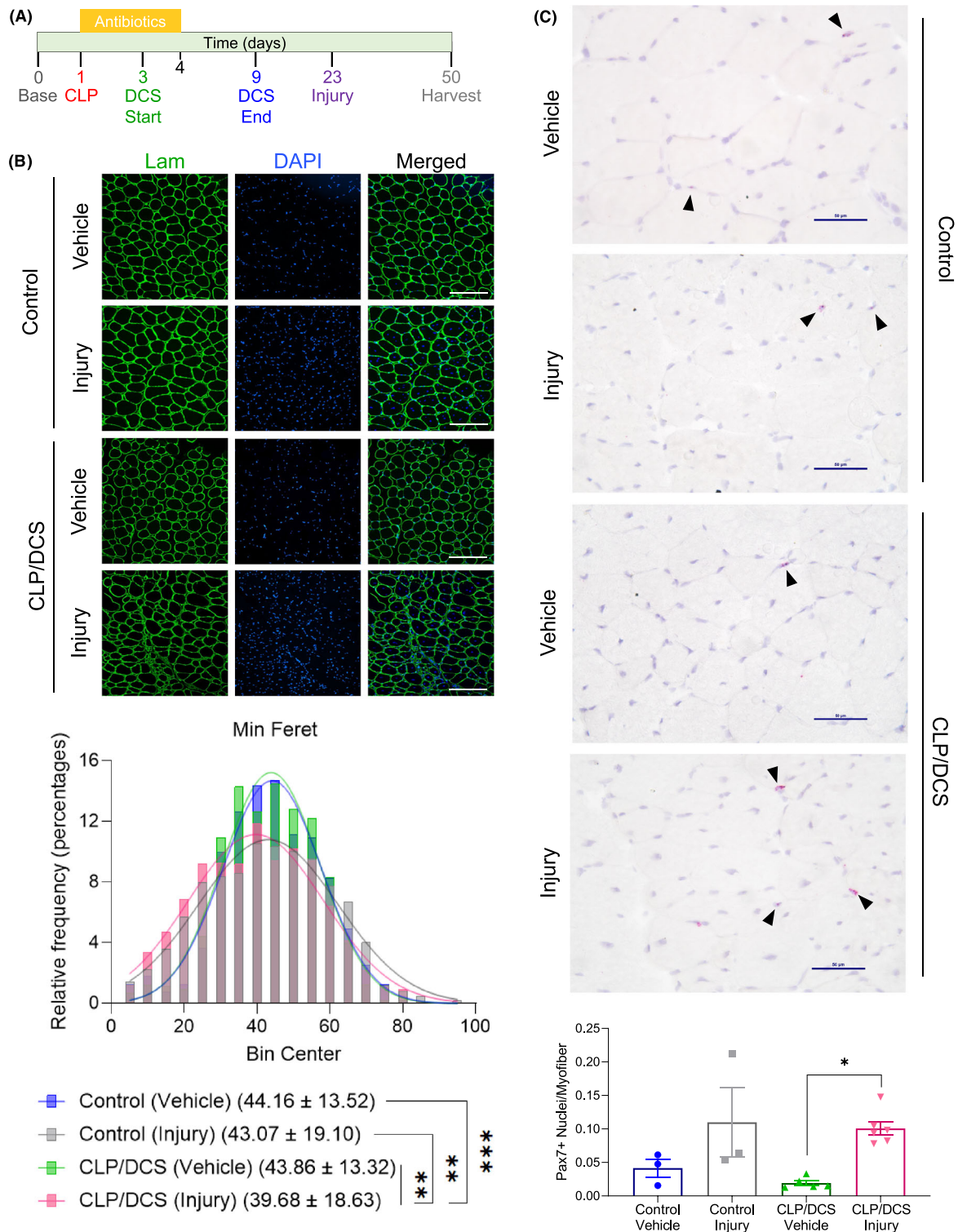


Figure 4 Muscle recovery deficit in post-sepsis mice with secondary muscle injury. (A) Timeline depicting experimental setup of second insult to muscle in control and cecal ligation and puncture/daily chronic stress (CLP/DCS) mice. (B) Immunofluorescence images (top) and minimum Feret diameter quantification (bottom) of tibialis anterior (TA) cross-sections in control or CLP/DCS mice that received vehicle or BaCl₂ (injured) injections. Green = laminin, Blue = DAPI. Images are $\times 20$ with scale bar = 200 μm . (C) Pax7 staining (top) and quantification of Pax7-positive nuclei per myofibre of TA cross-sections from vehicle or injured control and CLP/DCS mice. Purple = haematoxylin (nuclei), Red = Pax7. Images are $\times 40$ with scale bar = 50 μm . All images are representative. B = nonlinear fit pairwise comparisons, see Table S6 for all P values from all comparisons. C = One-way ANOVA with Bonferroni multiple comparisons (BMC). Significance is $*P < 0.05$, $**P < 0.01$, $***P < 0.001$. $N = 3-6$. Each $n =$ one mouse.

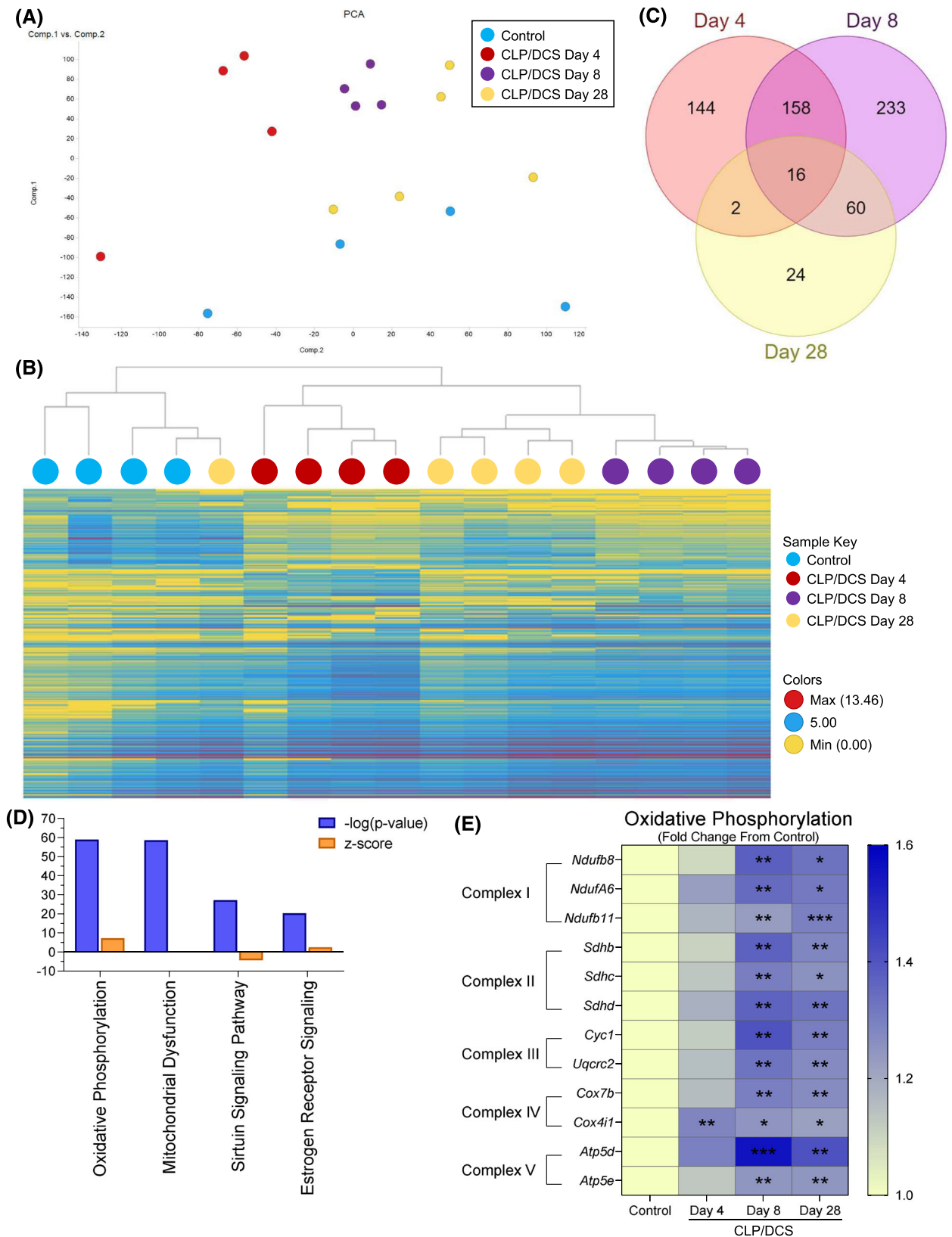


Figure 5 Post-septic satellite cell RNA seq reveals metabolic defects potential contributions to long term functional deficits. Combined experiment (A) principal component analysis (PCA) of control and cecal ligation and puncture/daily chronic stress (CLP/DCS) Days 4, 8 and 28 utilizing all gene transcriptomic data. (B) Hierarchical clustering by means of combined differentially expressed genes from CLP/DCS Days 4, 8 and 28 versus control using $2 < \text{Log}_2\text{FC} < -2$, $P < 0.05$. (C) Venn diagram illustrating the overlap in significantly altered genes in CLP/DCS Days 4, 8 and 28 samples versus control, where $2 < \text{Log}_2\text{FC} < -2$, $P < 0.05$. (D) Top 4 altered pathways from ingenuity pathway analysis (IPA) in CLP/DCS Day 28 versus control samples. Orange bars indicate z-score, blue bars indicate $-\log(P\text{-value})$. (E) Heatmap of significantly altered oxidative phosphorylation genes in CLP/DCS Day 28 versus control (depicted as Log_2 transcript expression [FPKM] of CLP/DCS Days 4, 8 and 28 as a fold change from control) that are represented in more than one of the top 4 altered pathways from IPA; Ndufa6, Ndufb8 transcript variant 1, Ndufb11, Sdhb, Sdhc, Sdhd, Cyc1, Uqcrc2, Cox4i1 transcript variant 1, Cox7b, Atp4d transcript variant 2 and Atp5e. Significance indicated is versus control. *B* = Clustering method: complete linkage; distance measure: correlation. *E* = One-way ANOVA with Bonferroni multiple comparisons (BMC) whereby significance is * $P < 0.05$, ** $P < 0.01$, *** $P < 0.001$. $n = 4\text{--}5$. Each n = pooled satellite cells isolated from 2–3 mice. Satellite cells harvested from mice on Day 27 or 28 are labelled as Day 28.

lites (including amino acids) that are found increased in septic patient serum/plasma or in septic non-survivors compared with survivors³⁶ are also increased in CLP/DCS muscle (Figure 6C).

We next analysed the top up- and down-regulated metabolites for each CLP/DCS time point versus control (see top 10 differentially abundant metabolites in Figure S9) in MetaboAnalyst to determine the top altered metabolic pathways in CLP/DCS Days 4, 8 and 28 (Figures S10A–C). Although there are some potential indicators that mitochondrial function is altered during these time points (e.g., nicotinate and nicotinamide metabolism and beta oxidation of very long chain fatty acids), a clear mitochondrial metabolism deficit was not observed. Further, metabolites more specifically related to mitochondrial function—such as oxidative phosphorylation (Figure 6D) and the tricarboxylic acid cycle (Figure 6E)—did not reveal clear changes indicative of sustained mitochondrial dysfunction. These data suggest that the altered mitochondrial signature found in satellite cells is likely not a simple reflection or consequence of widespread whole muscle mitochondria defects.

Discussion

Many sepsis survivors suffer from long-term health consequences that significantly compromise quality of life. Currently, there are few treatments available addressing these chronic issues. Understanding how tissues/organs are lastingly impacted by sepsis is of high clinical importance given the growing number of sepsis cases/sepsis survivors worldwide. To this end, numerous studies have investigated the detrimental role of sepsis on skeletal muscle and other organs/tissues such as adipose tissue and the gut microbiome.^{37–39} That said, the majority of studies to date evaluated the effect of sepsis on these tissues/organs during a very narrow post-sepsis timeframe that failed to capture long-term sequelae. This lack of extended post-sepsis follow-up highlights a major gap in the field, especially considering that molecular changes associated with acute and late sepsis phases are distinct. For example, a previous study recently characterized changes in the microenvironment of mu-

rine skeletal muscle and adipose tissue at one day and one month post-sepsis.³⁸ While patterns of cell type abundance shifts were observed across many cell types in both tissues, closer examination revealed natural killer cells and T-memory cells in one month post-sepsis samples, whereas T-regulatory and T-memory cells characterized immune cell diversity in one month post-sepsis adipose tissue. Notably, none of these populations were appreciably present in control or 1 day post-sepsis mice.³⁸ While just one example, these data highlight that post-sepsis tissue microenvironment remodelling is tissue specific and that acute and chronic phases are dynamic and distinct.

A number of tissue stem cell populations are known to be impacted during and following sepsis. Zhang *et al.* demonstrated that lipopolysaccharide activates the Toll-like receptor 4 (TLR4) in haematopoietic stem cells (HSCs) [S1]. Subsequently, two downstream pathways of TLR4, myeloid differentiation factor 88 (MYD88) and TIR-domain-containing adapter-inducing interferon β (TRIF) are activated [S1]. Each of these pathways uniquely impacts overall stem cell function, whereby MYD88 causes myelosuppression and TRIF causes persistent injury to the HSC population [S1]. Furthermore, we previously showed a significant loss of adipose stem cells in both 1-day and 1-month post-septic mice.³⁸ These findings implicate widespread post-sepsis stem cell disruption that may contribute to adverse, long-term consequences of tissue dysfunction. As muscle wasting is observed in both human sepsis^{13,14} and animal models of sepsis²³ [S2], we sought to query the impact of sepsis on skeletal muscle stem cells. Our study is the first to demonstrate the necessity of muscle stem cells for full recovery of lean mass in a murine surgical model of sepsis. Although our results are not the first to implicate metabolic defects in the post-sepsis satellite cell population [S3], it is the first study that reports an unbiased longitudinal assessment of the satellite cell transcriptome from post-septic mice.

We observed a substantial number of transcripts encoding proteins of mitochondrial complexes I–V within the top 4 altered pathways (oxidative phosphorylation, mitochondrial dysfunction, sirtuin signalling pathway, and oestrogen receptor signalling) in CLP/DCS Day 28 versus control satellite cells. As metabolic state is important for proper cell function, this metabolic switch in post-septic satellite cells—in conjunction

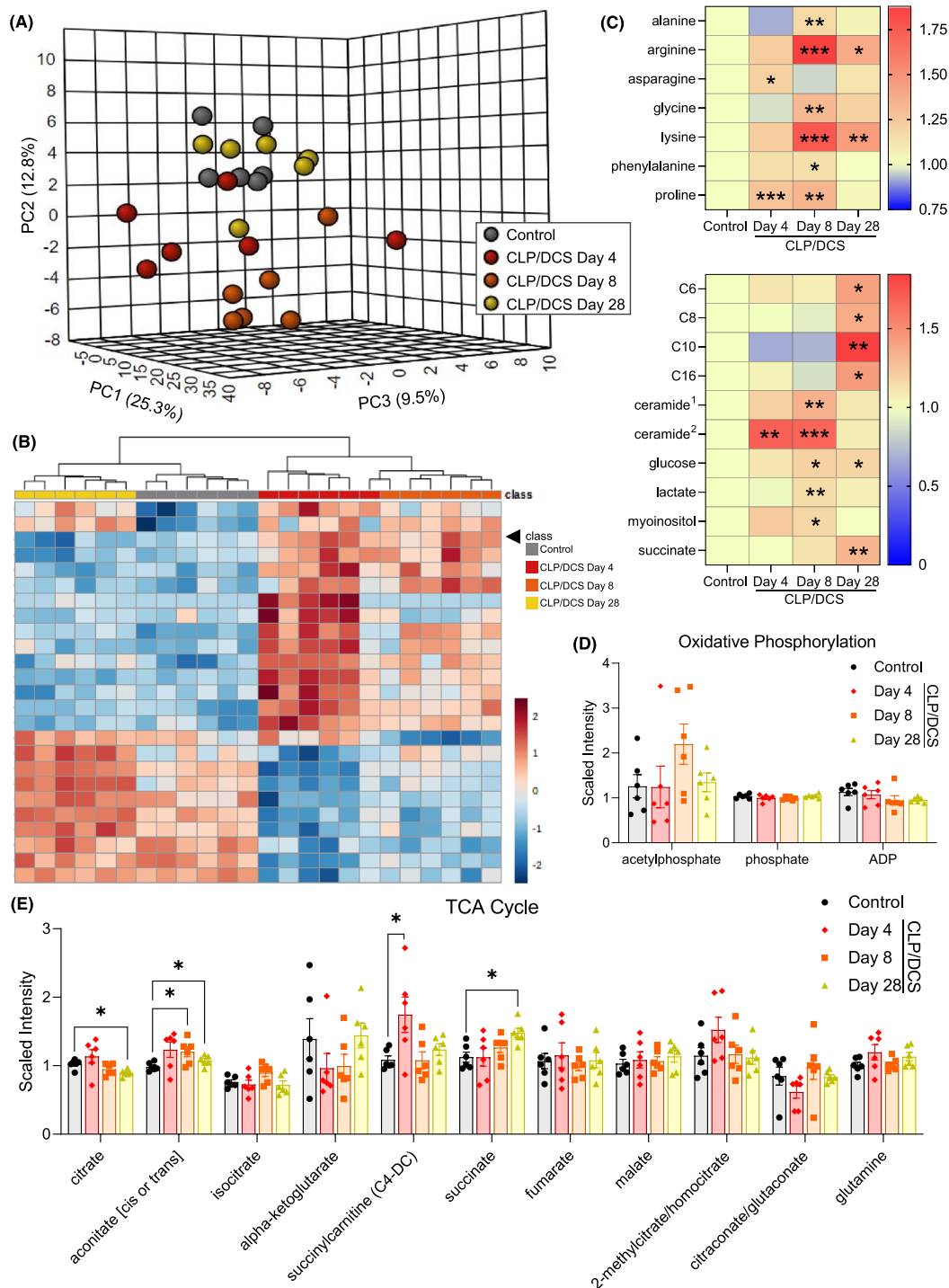


Figure 6 Alterations in post-septic gastrocnemius metabolites do not align with metabolic changes observed in satellite cells. (A) 3D principal component analysis (PCA) plot (MetaboAnalyst) utilizing all control, Days 4, 8 and day 28 cecal ligation and puncture/daily chronic stress (CLP/DCS) gastrocnemius metabolite levels. (B) Hierarchical clustering (MetaboAnalyst) of control, CLP/DCS days 4, 8 and 28 using the top 25 altered metabolites. (C) Heatmap depicting increased scaled intensity values, as fold change from control, of metabolites in CLP/DCS gastrocnemius (GR) that are also increased in serum/plasma of septic versus healthy patients or increased in non-surviving versus surviving sepsis patients. Significance indicated is versus control values. (D, E) Scaled intensity levels of metabolites involved in oxidative phosphorylation (D) or the tricarboxylic acid (TCA) cycle (E) in control, Days 4, 8 and 28 CLP/DCS mice. GR muscles that were harvested on Day 27 or 28 are labelled as Day 28. B = Clustering method: complete; distance measure: Euclidean. C–E = Student’s unpaired t-test with Welch’s correction (Metabolon). Significance is **P* < 0.05, ***P* < 0.01, ****P* < 0.001. *N* = 6 per group. Each *n* = one mouse. C6, hexanoylcarnitine; C8, octanoylcarnitine; C10, decanoylcarnitine; C16, palmitoylcarnitine; ceramide¹, ceramide (d18:1/14:0, d16:1/16:0); ceramide², ceramide (d18:2/24:1, d18:1/24:2).

with changes in satellite cell morphology and decreased proliferation (*Figure 3D*)—suggests a potential connection between these molecular observations and satellite cell dysfunction. Further investigation is certainly needed to address this potential relationship. Additionally, metabolism is tightly linked to overall muscle function, regeneration and disease [S4–S6]. Examples include key roles for oxidative phosphorylation and oxidative stress in muscle disease aetiology (i.e., DMD) [S7] as well as muscle stem cell fate decisions [S8]. Moreover, multiple studies show that targeting mitochondrial metabolic dysfunction can improve disease severity and/or outlook. First, in diabetic and obese mouse models for example, activation of mitochondrial glycerol 3-phosphate dehydrogenase, the rate-limiting step in the glycerophosphate shuttle, improved muscle regeneration parameters (increased myofibre cross-sectional area, increased number of myofibres with centrally located nuclei and increased expression of myogenin) as well as increasing overall muscle weight [S9]. Second, a recent cancer cachexia study reported increased fatty acid oxidation in the muscle resulting from proinflammatory signals that led to increased oxidative stress and p38MAPK stress signalling [S10]. Treatment of tumour-bearing mice with etomoxir, an inhibitor of fatty acid oxidation, improved body weight, increased muscle cross sectional area and increased myosin heavy-chain expression [S10]. Third, a small clinical trial involving adults with Becker muscular dystrophy found that treatment with (–)-epicatechin was able to increase mitochondrial biogenesis markers, skeletal muscle growth markers and markers of skeletal muscle regeneration [S11]. These and other studies, combined with our findings reported here, underscore the importance of understanding foundational principles of how metabolism, satellite cells and muscle homeostasis are impacted by various stressors, including sepsis.

While, our study is an important step towards understanding the role of satellite cells in post-sepsis muscle recovery, there are some limitations to consider. First, our animal studies were performed predominantly using female mice, and thus, sex differences were not able to be queried here. Some previous human studies indicate that females may have increased sepsis survivability [S12, S13], which led us to initially use female mice. Nonetheless, future rigorous investigation into the male response is needed. Second, food intake and activity were not taken into consideration in our results, leading to the potential that these variables could play a role in selected study outcomes. Lastly, we used the TA muscle for histology (i.e., myofibre typing and minimum Feret diameter measurements) and GR for metabolomics which may not be completely reflective of all types of skeletal muscle responses to sepsis in the hindlimb from which satellite cells were isolated. Further studies would be needed addressing the long-term effect of sepsis on additional skeletal muscle types both in the hindlimb and in other anatomical locations. Even with such limitations, new hypotheses for the role of satellite

cells in sepsis-related atrophy recovery and the effect of sepsis on satellite cells can be gleaned. As mentioned above, we hypothesize that the transcriptional changes in satellite cells (likely representing an altered metabolic state) is leading to functional satellite cell deficits (i.e., reduced proliferation and morphology changes, *Figure 3*). Thus, post-septic mice (even if ostensibly ‘recovered’) harbour a compromised satellite cell pool making them susceptible to future muscle loss or even the ability to completely recover pre-sepsis lean mass levels (*Figure 4*). Understanding why these changes persist in satellite cells is an important question, but at the very least, these changes do not appear to be caused by myofibre type switching or as a consequence of whole muscle mitochondrial dysfunction.

Muscle wasting is associated with sepsis mortality,¹⁵ and thus preventing and/or rescuing muscle wasting outcomes may help further improve sepsis survivability. In addition to survivability, improving self-reliance, the ability to perform daily activities, and/or to maintain employment would (1) increase overall quality of life and (2) likely reduce the number of sepsis survivors that develop depression, as losing independence and income is likely to lead to unhappiness and/or discontent. Future work would benefit from studies of how these deficits in muscle regeneration post-sepsis is affected by age and/or other comorbidities (such as obesity and diabetes) as the aged population, ≥ 65 years, accounts for 40% of sepsis cases and tend to have a more severe reaction (i.e., higher SOFA scores than other ages) and worse outcome (i.e., death and disability) [S14].

The value of targeting muscle wasting during and following sepsis is clear. A key outstanding question is how to best target disease or trauma-associated muscle wasting. Targeting/limiting muscle catabolism is one approach that is popular among many in the muscle wasting field. On the other hand, boosting and/or promoting muscle regeneration (via stem cell manipulation or modulation of the muscle microenvironment) is gaining traction as a way to not necessarily eliminate, prevent or reverse muscle wasting, but rather to slow the rate of atrophy or accelerate recovery. While this study confirmed and highlighted the key role of muscle stem cells during sepsis recovery, next steps include determining how to best manipulate this cell compartment/the regenerative process without interfering with other recovery/repair processes in other affected tissues. If successful, a regenerative medicine-based approach may indeed be a powerful way to limit long-term chronic illness and improve the lives of countless sepsis survivors.

Acknowledgements

The authors would like to thank Genewiz, LLC, for their services for RNA sequencing and Metabolon Inc. for performing

the whole muscle untargeted metabolomics. In addition, the authors appreciate all past and present members of the Doles lab for their helpful discussions and suggestions regarding this manuscript. The authors of this manuscript certify that they comply with the ethical guidelines for authorship and publishing in the *Journal of Cachexia, Sarcopenia and Muscle*.⁴⁰

Funding

We acknowledge the following funding sources for this work: National Institute of General Medical Sciences (5R35GM128594-04) to JDD; NIAMS Musculoskeletal Research Training Program (T32AR56950) to RES.

References

- Singer M, Deutschman CS, Seymour CW, Shankar-Hari M, Annane D, Bauer M, et al. The Third International Consensus Definitions for Sepsis and Septic Shock (Sepsis-3). *JAMA* 2016;**315**:801–810.
- Rudd KE, Johnson SC, Agesa KM, Shackelford KA, Tsoi D, Kievlan DR, et al. Global, regional, and national sepsis incidence and mortality, 1990–2017: analysis for the Global Burden of Disease Study. *Lancet* 2020;**395**:200–211.
- Hawkins RB, Raymond SL, Stortz JA, Horiguchi H, Brakenridge SC, Gardner A, et al. Chronic critical illness and the persistent inflammation, immunosuppression, and catabolism syndrome. *Front Immunol* 2018;**9**:1511.
- Gentile LF, Cuenca AG, Efron PA, Ang D, Bihorac A, McKinley BA, et al. Persistent inflammation and immunosuppression: a common syndrome and new horizon for surgical intensive care. *J Trauma Acute Care Surg* 2012;**72**:1491–1501.
- Mira JC, Gentile LF, Mathias BJ, Efron PA, Brakenridge SC, Mohr AM, et al. Sepsis pathophysiology, chronic critical illness, and persistent inflammation-immunosuppression and catabolism syndrome. *Crit Care Med* 2017;**45**:253–262.
- Mankowski RT, Anton SD, Ghita GL, Brumback B, Darden DB, Bihorac A, et al. Older adults demonstrate biomarker evidence of the persistent inflammation, immunosuppression, and catabolism syndrome (PICS) after sepsis. *J Gerontol A Biol Sci Med Sci* 2022;**77**:188–196.
- Rosenthal MD, Moore FA. Persistent inflammatory, immunosuppressed, catabolic syndrome (PICS): a new phenotype of multiple organ failure. *J Adv Nutr Hum Metab* 2015;**1**.
- Battle CE, Davies G, Evans PA. Long term health-related quality of life in survivors of sepsis in South West Wales: an epidemiological study. *PLoS ONE* 2014;**9**:e116304.
- Cuthbertson BH, Elders A, Hall S, Taylor J, MacLennan G, Mackirdy F, et al. Mortality and quality of life in the five years after severe sepsis. *Crit Care* 2013;**17**:R70.
- Winters BD, Eberlein M, Leung J, Needham DM, Pronovost PJ, Sevransky JE. Long-term mortality and quality of life in sepsis: a systematic review. *Crit Care Med* 2010;**38**:1276–1283.
- Opal SM, Laterre PF, Francois B, LaRosa SP, Angus DC, Mira JP, et al. Effect of eritoran, an antagonist of MD2-TLR4, on mortality in patients with severe sepsis: the ACCESS randomized trial. *JAMA* 2013;**309**:1154–1162.
- Yende S, Austin S, Rhodes A, Finfer S, Opal S, Thompson T, et al. Long-term quality of life among survivors of severe sepsis: analyses of two international trials. *Crit Care Med* 2016;**44**:1461–1467.
- Callahan LA, Supinski GS. Sepsis-induced myopathy. *Crit Care Med* 2009;**37**:S354–S367.
- Mankowski RT, Laitano O, Clanton TL, Brakenridge SC. Pathophysiology and treatment strategies of acute myopathy and muscle wasting after sepsis. *J Clin Med* 2021;**10**:1874.
- Lee Y, Park HK, Kim WY, Kim MC, Jung W, Ko BS. Muscle mass depletion associated with poor outcome of sepsis in the emergency department. *Ann Nutr Metab* 2018;**72**:336–344.
- Prescott HC, Angus DC. Enhancing recovery from sepsis: a review. *JAMA* 2018;**319**:62–75.
- Yin H, Price F, Rudnicki MA. Satellite cells and the muscle stem cell niche. *Physiol Rev* 2013;**93**:23–67.
- Arneson PC, Doles JD. Impaired muscle regeneration in cancer-associated cachexia. *Trends Cancer* 2019;**5**:579–582.
- Zhang L, Wang XH, Wang H, du J, Mitch WE. Satellite cell dysfunction and impaired IGF-1 signaling cause CKD-induced muscle atrophy. *J Am Soc Nephrol* 2010;**21**:419–427.
- Yamakawa H, Kusumoto D, Hashimoto H, Yuasa S. Stem cell aging in skeletal muscle regeneration and disease. *Int J Mol Sci* 2020;**21**:1830.
- Wang YX, Feige P, Brun CE, Hekmatnejad B, Dumont NA, Renaud JM, et al. EGFR-Aurka signaling rescues polarity and regeneration defects in dystrophin-deficient muscle stem cells by increasing asymmetric divisions. *Cell Stem Cell* 2019;**24**:419–432 e6.
- Price FD, von Maltzahn J, Bentzinger CF, Dumont NA, Yin H, Chang NC, et al. Inhibition of JAK-STAT signaling stimulates adult satellite cell function. *Nat Med* 2014;**20**:1174–1181.
- Owen AM, Patel SP, Smith JD, Balasuriya BK, Mori SF, Hawk GS, et al. Chronic muscle weakness and mitochondrial dysfunction in the absence of sustained atrophy in a preclinical sepsis model. *Elife* 2019;**8**:8.
- Minnaard R, Drost MR, Wagenmakers AJ, Van Kranenburg GP, Kuipers H, Hesselink MK. Skeletal muscle wasting and contractile performance in septic rats. *Muscle Nerve* 2005;**31**:339–348.
- Stortz JA, Hollen MK, Nacionales DC, Horiguchi H, Ungaro R, Dirain ML, et al. Old mice demonstrate organ dysfunction as well as prolonged inflammation, immunosuppression, and weight loss in a modified surgical sepsis model. *Crit Care Med* 2019;**47**:e919–e929.
- Murphy MM, Lawson JA, Mathew SJ, Hutcheson DA, Kardon G. Satellite cells, connective tissue fibroblasts and their interactions are crucial for muscle regeneration. *Development* 2011;**138**:3625–3637.
- Osuchowski MF, Ayala A, Bahrami S, Bauer M, Boros M, Cavillon JM, et al. Minimum Quality Threshold in Pre-Clinical Sepsis Studies (MQTiPSS): an international expert consensus initiative for improvement of animal modeling in sepsis. *Shock* 2018;**50**:377–380.
- Wen Y, Murach KA, Vechetti II Jr, Fry CS, Vickery C, Peterson CA, et al. MyoVision:

Conflict of interest

The authors have no conflicts of interest to disclose.

Online supplementary material

Additional supporting information may be found online in the Supporting Information section at the end of the article.

- software for automated high-content analysis of skeletal muscle immunohistochemistry. *J Appl Physiol (1985)* 2018;**124**:40–51.
29. Schneider CA, Rasband WS, Eliceiri KW. NIH Image to ImageJ: 25 years of image analysis. *Nat Methods* 2012;**9**:671–675.
30. Joseph J, Cho DS, Doles JD. Metabolomic analyses reveal extensive progenitor cell deficiencies in a mouse model of Duchenne muscular dystrophy. *Metabolites* 2018;**8**:61.
31. Kramer A, Green J, Pollard J Jr, Tugendreich S. Causal analysis approaches in ingenuity pathway analysis. *Bioinformatics* 2014;**30**:523–530.
32. Pang Z, Chong J, Zhou G, de Lima Morais DA, Chang L, Barrette M, et al. MetaboAnalyst 5.0: narrowing the gap between raw spectra and functional insights. *Nucleic Acids Res* 2021;**49**:W388–W396.
33. Chen X, Li X, Lu H, Xu Y, Wei Y, Cao K, et al. Mouse model of critical persistent inflammation, immunosuppression, and catabolism syndrome. *Shock* 2022;**57**:238–245.
34. Pova P, Coelho L, Almeida E, et al. C-reactive protein as a marker of infection in critically ill patients. *Clin Microbiol Infect* 2005;**11**:101–108.
35. Ferrario M, Pastorelli R, Brunelli L, Liu S, Zanella do Amaral Campos PP, Casoni D, et al. Persistent hyperammonia and altered concentrations of urea cycle metabolites in a 5-day swine experiment of sepsis. *Sci Rep* 2021;**11**:18430.
36. Hussain H, Vutipongsatorn K, Jimenez B, et al. Patient stratification in sepsis: using metabolomics to detect clinical phenotypes, sub-phenotypes and therapeutic response. *Metabolites* 2022;**12**:376.
37. Zanders L, Kny M, Hahn A, Schmidt S, Wundersitz S, Todiras M, et al. Sepsis induces interleukin 6, gp130/JAK2/STAT3, and muscle wasting. *J Cachexia Sarcopenia Muscle* 2022;**13**:713–727.
38. Cho DS, Schmitt RE, Dasgupta A, Ducharme AM, Doles JD. Single-cell deconstruction of post-sepsis skeletal muscle and adipose tissue microenvironments. *J Cachexia Sarcopenia Muscle* 2020;**11**:1351–1363.
39. Adelman MW, Woodworth MH, Langelier C, Busch LM, Kempker JA, Kraft CS, et al. The gut microbiome's role in the development, maintenance, and outcomes of sepsis. *Crit Care* 2020;**24**:278.
40. von Haehling S, Morley JE, Coats AJS, Anker SD. Ethical guidelines for publishing in the Journal of Cachexia, Sarcopenia and Muscle: update 2021. *J Cachexia Sarcopenia Muscle* 2021;**12**:2259–2261.